The Journal of Chemical Physics

An investigation of the sites occupied by atomic barium in solid xenon—A 2D-EE luminescence spectroscopy and molecular dynamics study

Cite as: J. Chem. Phys. **148**, 124308 (2018); https://doi.org/10.1063/1.5019890
Submitted: 18 December 2017 . Accepted: 07 March 2018 . Published Online: 27 March 2018

Barry M. Davis, Benoit Gervais, and John G. McCaffrey

An investigation of the sites occupied by atomic barium in solid xenon—A 2D-EE luminescence spectroscopy and molecular dynamics study

Barry M. Davis,[1] Benoit Gervais,[2] and John G. McCaffrey[1,a)]
[1]*Department of Chemistry, Maynooth University, National University of Ireland–Maynooth, County Kildare, Ireland*
[2]*Normandie Université, ENSICAEN, UNICAEN, CEA, CNRS, CIMAP, 14000 Caen, France*

(Received 18 December 2017; accepted 7 March 2018; published online 27 March 2018)

A detailed characterisation of the luminescence recorded for the 6p $^1P_1$–6s $^1S_0$ transition of atomic barium isolated in annealed solid xenon has been undertaken using two-dimensional excitation–emission (2D-EE) spectroscopy. In the excitation spectra extracted from the 2D-EE scans, two dominant thermally stable sites were identified, consisting of a classic, three-fold split Jahn-Teller band, labeled the blue site, and an unusual asymmetric 2 + 1 split band, the violet site. A much weaker band has also been identified, whose emission is strongly overlapped by the violet site. The temperature dependence of the luminescence for these sites was monitored revealing that the blue site has a non-radiative channel competing effectively with the fluorescence even at 9.8 K. By contrast, the fluorescence decay time of the violet site was recorded to be 4.3 ns and independent of temperature up to 24 K. The nature of the dominant thermally stable trapping sites was investigated theoretically with Diatomics-in-Molecule (DIM) molecular dynamics simulations. The DIM model was parameterized with *ab initio* multi-reference configuration interaction calculations for the lowest energy excited states of the Ba·Xe pair. The simulated absorption spectra are compared with the experimental results obtained from site-resolved excitation spectroscopy. The simulations allow us to assign the experimental blue feature spectrum to a tetra-vacancy trapping site in the bulk xenon *fcc* crystal—a site often observed when trapping other metal atoms in rare gas matrices. By contrast, the violet site is assigned to a specific 5-atom vacancy trapping site located at a grain boundary. *Published by AIP Publishing.*
https://doi.org/10.1063/1.5019890

I. INTRODUCTION

Considerable interest currently exists in the photophysics of atomic barium isolated in solid xenon (Ba/Xe) principally because of the direct relevance of this system in the ***n***EXO project[1] as a method for the detection of the neutrinoless, double beta decay of ^{136}Xe to form ^{136}Ba di-cation. In connection with this work, Ba/Xe has been proposed as a matrix system that offers the potential for achieving single atom spectroscopy. The group at Maynooth has conducted a detailed study on the luminescence of the three Ba/RG (RG = Ar, Kr, and Xe) matrix systems and given the current level of interest in Ba/Xe, the results of this system alone will be presented here. More complete details of the sample preparation and treatments of this and the two other matrix (Ba/Ar and Ba/Kr) systems will be presented in an article currently being prepared in addition to a review of all three systems. Another reason for presenting the Ba/RG matrix results in this way is that, as will be shown ahead, the luminescence of the Ba/Xe system exhibits a pronounced temperature dependence while those observed for the other two hosts do not. Non-radiative decay of the $^1P_1$ state of atomic barium isolated in the dominant blue site of xenon may diminish the usefulness of this system as a candidate for single atom spectroscopy.

The emission spectroscopy of Ba/Xe has recently been reported by Fairbank and co-workers using CW laser excitation.[1] In that study complex emission bands were reported, which showed a strong dependence on sample preparation and treatments. In the current study, we focus attention on identifying the thermally stable sites of isolation and record the emission with two dimensional-excitation and emission (2D-EE) spectroscopy, to obtain the total luminescence of the system. Nanosecond time-resolved spectroscopy is then used to probe the excited state dynamics of atomic barium in all the sites identified. In a recent study,[2] we used absorption spectroscopy to characterise matrix-isolated atomic barium and distinguish it from barium clusters and strontium impurities. We also conducted quantum chemical calculations of the ground electronic states of nine M·RG diatomics to analyze the possible site occupancies of the metal atoms (M = Ba, Sr, and Ca) in the solid rare gases (RG = Ar, Kr, and Xe).

Inspection of the experimental Ba/Xe excitation scans, the details of which will be presented ahead, shows an unexpected and remarkable feature for one particular site. Thus, the violet site has a single peak on the low energy side, well separated from a double peak on the high energy side. This

a)Email: john.mccaffrey@mu.ie

is exactly the opposite of the spectral shape associated with the trapping of barium atoms on the surface of a cluster,[3] for which a double peak is observed on the low energy-side and a single peak on the high-energy side. Such an asymmetric feature suggests an elongated trapping site characterized by one long axis, along which the excited electronic cloud can expand nearly freely, and two short axes, along which the excited electronic cloud is confined. To probe the nature of this unusual site but also the more conventional symmetric, threefold-split band, we have undertaken molecular dynamics calculations to simulate the excitation bands and thereby gain insights into the nature of these very distinct spectral band shapes, both of which arise from thermally stable trapping sites.

The search to identify the trapping sites of barium atoms in solid xenon is determined by several considerations. As outlined in our previous work[2] on matrix-isolated atomic barium, sites have to be large enough to accommodate the large, spherical $(6s^2)^1S_0$ Ba atom without extensive distortion of the lattice. Recent coupled-cluster calculations[2] have shown that the ground state equilibrium inter-nuclear distance of the Ba·Xe pair is close to 5.55 Å, while the nearest neighbor distance in solid xenon is only 4.33 Å. Because of this size mismatch, single, double, and triple vacancy sites—as well as all interstitial sites—can, therefore, be excluded since they produce very cramped geometries that are energetically unfavorable. By contrast, the tetravacancy TV-T_d site, with the nearest Xe neighbors located at 5.08 Å before relaxation, is much more favorable. Very limited distortion of the matrix results in the Ba impurity occupying this site. The HV-O_h site, obtained by trapping the Ba atom in the middle of the *fcc* unit-cell and removing the 6 nearest Xe atoms, produces a high symmetry site, for which the nearest Xe neighbors are located at 5.35 Å without relaxation. The Ba atom fits even better[2] into this site. However, the energy balance between the TV-T_d and the HV-O_h sites is less favorable for the larger site because more Xe atoms are missing and the corresponding cohesion energy in the total energy of the matrix is thereby reduced. These two high symmetry crystalline trapping sites produce well-defined Jahn-Teller (JT) splitting, as observed for the blue site in Ba/Xe and possibly the green site, but they are unable to explain the highly asymmetric (2 + 1) profile observed for the excitation spectrum of the violet site.

Other kinds of trapping sites are possible, if we broaden the search to consider not only the perfect *fcc* lattice but also crystal defects. The matrix deposition leads to the formation of small crystal grains as observed by X-rays diffraction[4,5] and also indirectly by ESR measurements of K atoms trapped in the Ar matrix.[6] A limited fraction of these grains may have a *hcp* structure.[4] The interface region of these grains can offer alternative trapping sites as investigated for alkali atoms.[7] It is worth noting that the energy difference between the compact face centered cubic and hexagonal stacking is very small for rare gas crystals.[8,9] This favors the occurrence of stacking faults during the crystal growth and annealing. Such defects were actually observed for Xe matrices and other related trapping matrices.[8,9] The possibility of stacking faults or *hcp* environment was suggested to interpret the infrared spectrum of CCl_4 trapped in the Kr matrix.[10] There are also numerous examples from physical metallurgy[11,12] as illustrated in the case of Aluminum *fcc* lattice studies.[13] From a qualitative point of view, the grain boundaries are thermodynamically stable when the mismatch between the crystal parts of the grain is limited, rendering these trapping sites thermally stable up to some temperature. The annealing often performed to analyze the most stable sites can, however, induce a sufficient mobility to allow impurity migration and recombination as observed for alkali atoms.[7,14] Moreover, the nature of the impurity can influence the stability of the trapping site.[5] We did not exhaustively consider the numerous possibilities of grain boundaries capable of accommodating a Ba atom but instead, we investigated one particular case, which exhibits spectral features that convincingly match the experimental results.

One such grain boundary was obtained from two *fcc* crystalline parts, symmetric to each other with respect to the (111) plane of a grain. The symmetry plane is thus the 111 layer of both grains, which match perfectly along this plane. This structure is often referred to as a twin stacking fault in the literature.[13] Very similar structures referred to as intrinsic or extrinsic stacking faults can be obtained by considering alternative plane stacking along the [111] direction, for which one or several (111) planes are missing. It should be noted that such stacking faults are rather common defects observed by electron microscopy in *fcc* crystals or by numerical simulation.[8,9,11–13] Such a structure keeps some symmetry inherited from the original *fcc* crystal and common with the *hcp* structure. In particular, C_3 symmetry is conserved in the direction perpendicular to the grain boundary. It is possible to obtain a 5V D_{3h} vacancy from such a structure, by removing 3 Xe atoms in the boundary plane and 1 atom on both sides of this plane. Such a trapping site is characterized by 3 nearest Xe atoms located at 5.00 Å and 12 second nearest neighbors at 5.60 Å. Its size is thus comparable to those of the TV-T_d and HV-O_h sites of the perfect crystal. The two nearest neighbor Xe shells are not strongly perturbed by the relaxation of the lattice and the trapping site is characterized by one long axis perpendicular to the boundary plane. It is actually quite similar to the TV-T_d trapping site as it can be considered as the merger of 2 such vacancies in the boundary plane.

The structure of the paper is as follows. Initially the results of annealing freshly deposited Ba/Xe samples are presented in the form of 2D-EE plots. Photophysical characteristics of the sites identified as thermally stable are then extracted and the temperature dependence of their luminescence are probed. After the experimental characterisation of the three thermally stable sites of isolation, a theoretical analysis is provided for the two dominant sites. This involves molecular dynamics simulations of the site-resolved excitation spectra. For this work, the Diatomics-in-Molecule (DIM) method was employed using *ab initio* multi-reference configuration interaction (MRCI) potentials for the lowest energy excited states of diatomic Ba·Xe. The calculated excited states are also examined in relation to the non-radiative relaxation observed to compete effectively with the $^1P_1$ state fluorescence of atomic barium in solid xenon.

II. METHODS

A. Experimental

The method used for the preparation of all the Ba/Xe samples analyzed in the present luminescence study is, with one exception, the same as that described elsewhere in our earlier absorption work[2] on matrix-isolated barium. The exception being the effort made to avoid strong re-absorption effects that distort the intensities of the recorded luminescence. Thus, matrix samples with high optical densities exhibit strong reabsorption, an effect which very significantly weakens the blue portions of the recorded emission. Of the three Ba/RG matrix systems, this effect is fortunately least severe in Ba/Xe. Nevertheless, all the data analyzed here were obtained from Ba/Xe samples deposited at 10 K with low metal fluxes, conditions that favour atomic isolation but also to keep the optical densities low. Samples were then annealed to remove thermally unstable sites. Two dimensional-excitation and emission (2D-EE) spectra were extensively used, allowing changes in the luminescence to be easily tracked, such as those arising from re-absorption and those that occur with matrix annealing. The 2D-EE plots were then used to identify all the emission bands originating from the thermally stable sites. In the 2D-EE spectra shown, the scatter from the excitation source used has been removed for presentation purposes. The removal of the excitation light produces a well-defined diagonal border, as shown in Fig. 1, on the short wavelength side of the recorded emission.

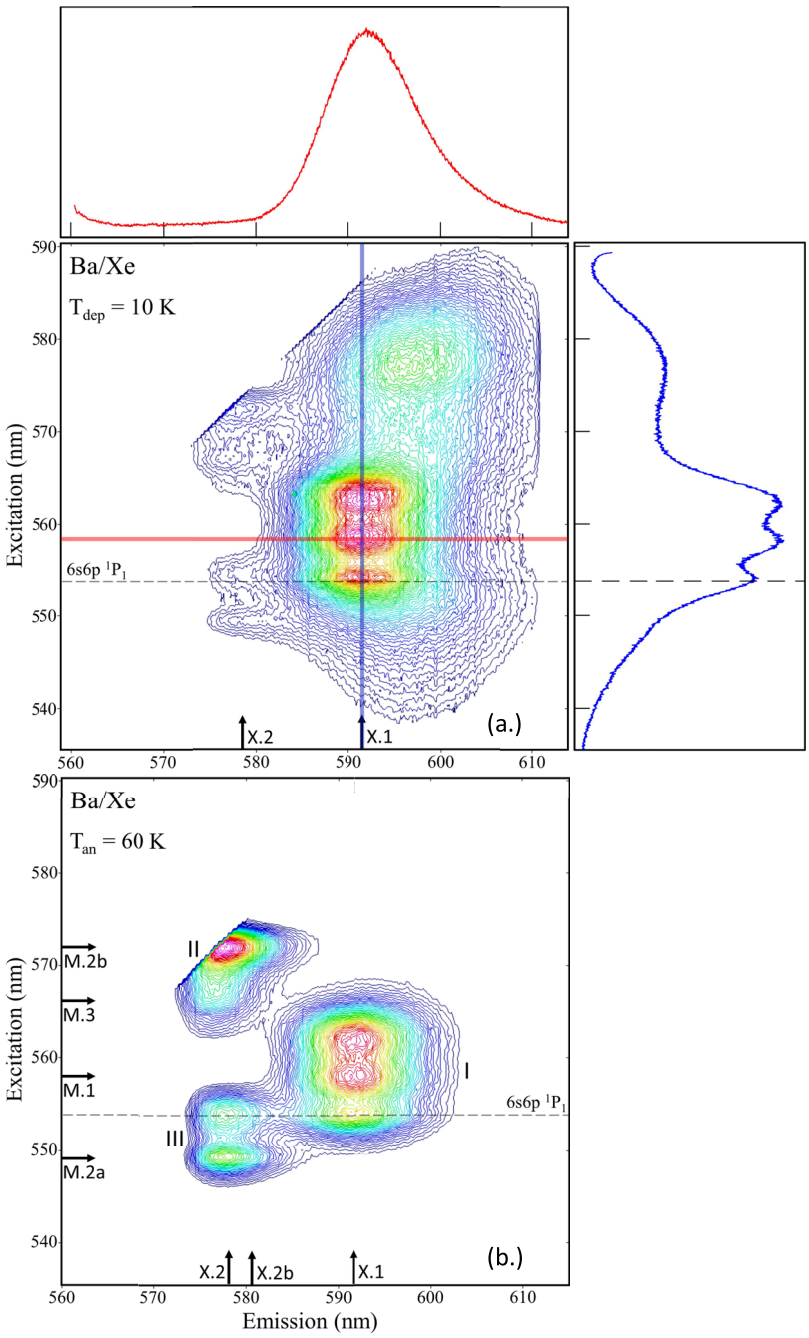

FIG. 1. Effects of annealing on the luminescence of atomic Ba isolated in Xe as manifested in two dimensional-excitation and emission (2D-EE) spectroscopy. These spectra were obtained with W-lamp excitation and CCD detection for a sample with an optical density of less than 0.5 at 560 nm. The upper panel presents the 2D-EE scan recorded for the entire (6s6p) $^1P_1$ luminescence of Ba/Xe following sample deposition at 10 K. A horizontal slice through the plot yields an emission spectrum (shown in red), whereas a vertical slice provides an excitation spectrum (X_1, shown in blue). The gas phase position of the (6s6p) $^1P_1 \leftarrow (6s^2)\ ^1S_0$ transition of Ba is indicated, in excitation only, as a dashed horizontal line. The 2D-EE spectrum recorded for the (6s6p) $^1P_1$ luminescence following sample annealing to 60 K is shown in the lower panel. Excitation and emission scans presented in the figures that follow and discussed in the text are indicated as X*n* and M*n*, respectively, on the 2D-EE plots.

Emission spectra were recorded perpendicular to the excitation beam with an Acton Research 0.5 m SP500i monochromator fitted with three gratings: a 1200 g/mm and a 150 g/mm both blazed at 300 nm and a 600 g/mm grating blazed at 500 nm. Two separate detectors were mounted on the SP500i: (1) A Hamamatsu R928P photomultiplier tube (PMT) maintained at −20 °C in Products for Research (Photocool, S600) cooled housing and (2) an intensified, time-gated charge coupled device (iCCD) detector (Andor Technologies, model iStar DH720) held at −15 °C using an integrated Peltier cooling system. A swing mirror in the SP500i allowed the emitted radiation to reach the detector of choice. For steady-state scans, the photomultiplier tube (PMT) was operated in photon counting mode by relaying its signal via an amplifier/discriminator module to the ARC NCL data acquisition and controller unit. The iCCD detector could also record time-integrated spectra by switching to its continuous-wave mode of operation. In this case, the Andor iStar software and card (CCI-010), mounted on a PC, controlled the SP-500i monochromator and selected the emission region of interest.

Nanosecond time-resolved luminescence spectra were recorded with pulsed excitation using a Q-switched Nd:YAG laser (Quantel, YG-980E-10) operating at a repetition rate of 10 Hz. The third harmonic of the YAG (355 nm) was used to pump a dye laser (Quantel, TDL-90), with Coumarin 540A as the dye, to produce tuneable laser radiation in the 523-586 nm range. Typical laser fluences in the range 2–6 $\mu J/mm^2$ were recorded in the sample window with a Molectron (Powermax 500 A) meter and PM10V1 head. These fluences were obtained using only the oscillator and pre-amplifier of the dye laser and varied in the range quoted, depending on the excitation wavelength selected. The resulting emission was detected with a time-gated iCCD camera and from the recorded time-resolved spectra, decay curves were extracted at selected emission wavelengths. Excited state lifetimes were obtained by fitting exponential functions (after re-convolution with the laser pulse) to the recorded emission decay curves.

B. Theoretical

A full *ab initio* simulation of the trapping of atomic barium in a solid rare gas matrix is a formidable computational challenge, so alternative methods must be used. A survey of the literature reveals that two distinct methods have been developed for single valence electron atoms. For the alkali series, trapped in light rare gas matrices, effective Hamiltonian models have been used with some success to assign the trapping sites or to perform non-adiabatic molecular dynamics.[7,15] For the majority of systems, however, where the use of a single-electron model cannot be generalized easily to more complex atoms, the Diatomic-in-molecule (DIM) method has been used most often.[16–19] The method has been used, in particular, to study the dynamics of CaAr[18] and BaAr.[19]

The DIM method is based on valence bond theory and is in principle exact, provided a sufficiently large configuration basis is used. In practice, this approach is further simplified by neglecting the configuration overlap and by truncating the basis set to its minimal representation. In its simplest version, neglecting inter-shell coupling, it can be obtained by means of degenerate first-order perturbation theory.[20] The Hamiltonian of the whole Ba/Xe system can, therefore, be formulated from the single Ba·Xe diatomic adiabatic energies combined with rotations, which allows the Hamiltonian associated with each Ba·Xe pair in the matrix sample to be expressed in a common, single frame. The DIM method is not expected to be quantitative in predicting the gas-to-matrix shift. However, the splitting of the triply degenerate ^{1}P states is often well reproduced by the DIM method.[16]

We have used such an approach for Ba/Xe in which the configuration space consists of the lowest energy spin singlet states of the Ba atom, i.e., the $6s^2(^1S)$, $6s5d(^1D)$, and $6s6p(^1P)$ states. Following previous DIM simulations done for numerous systems composed of a metal atom embedded in an ensemble of rare gas atoms, we have neglected here the inter-shell couplings. For the ^1S-^1P transition of interest, the model Hamiltonian equation used to compute the position-dependent energy is thus identical to the equation given explicitly in Refs. 16 and 20. It reduces to a 4×4 matrix made of a 1×1 block for the $6s^2(^1S)$ state and a 3×3 block for the $6s6p(^1P)$ states. The 5×5 block corresponding to the $6s5d(^1D)$ states is not coupled to the other blocks in our model and is not used in the present simulation. Spin-orbit coupling with the triplet states is neglected here. The reference potential energy curves (PEC) for the Ba·Xe dimer, including the ground state, were obtained by means of second-order configuration interaction (SOCI) including scalar relativistic correction, with a large ANO-RCC basis set.[21,22] The reference calculations were performed with the MOLCAS quantum chemistry package.[23] The equilibrium positions and well depths are summarized in Table I. The comparison of the ground state properties with those obtained by means of the more accurate coupled-cluster with full treatment of single and double excitations and perturbative triple excitations [CCSD(T)] calculation performed with the same basis set and basis set superposition error (BSSE) correction gives an indication regarding the accuracy of the SOCI reference potential used to parameterize the DIM method. The lack of core-core correlation of the SOCI method is rather obvious and results in a bond that is too soft. The SOCI calculations are also compared with results obtained by means of two different methods based on a valence configuration interaction combined with a core-polarization pseudopotential.[24,25] Our reference calculations give slightly shorter and deeper potential wells than those obtained in Ref. 25. The results of Ref. 24 give, on the contrary, bond lengths which are too short and potential wells which are too deep. Regarding the use of the SOCI for the DIM parameterization, they provide us with a consistent set of data and it must be emphasized that the exact position of the minima is not critical for these rather flat potential energy curves.

The search for the trapping sites of atomic barium in solid xenon and the generation of the simulated $6s6p(^1P)$ Ba/Xe absorption spectra were conducted using the method described in Ref. 7. Briefly, we first select a matrix structure, either the *fcc* crystal or a grain boundary, and generate a matrix sample consisting of approximately 600 atoms. We then remove a selected number of rare gas atoms and introduce the Ba atom inside the cavity created. The system is then relaxed for the ground state Ba atom by means of damped molecular dynamics until the equilibrium geometry associated with the initial guess

TABLE I. A summary of the Ba–Xe interaction potentials calculated in this study and used in the spectral simulations. The minimum positions (R_e) and well depths (D_e) are provided. More details about the calculations are provided in the supplementary material.

State	Ba atom asymptote	R_e (a.u.)	D_e (cm^{-1})	Method/reference
$1^1\Sigma^+$	$6s^2(^1S)$	11.4	75	SOCI[a]
		10.4	145	CCSD(T)[b]
		10.5	131	CCSD(T)[2]
		11.2	101	CPP[25]
		9.7	427	CPP[24]
$2^3\Pi$	$6s6p(^3P)$	9.4	164	SOCI[a]
		9.5	213	CPP[25]
		8.0	573	CPP[24]
$3^3\Sigma^+$	$6s6p(^3P)$	13.5	52	SOCI[a]
		15.5	22	CPP[25]
		13.0	30	CPP[24]
$2^1\Pi$	$6s6p(^1P)$	10.1	134	SOCI[a]
		10.7	130	CPP[25]
		7.8	817	CPP[24]
$3^1\Sigma^+$	$6s6p(^1P)$	14.3	34	SOCI[a]
		17.0	23	CPP[25]
		12.1	48	CPP[24]

[a]In this work, the SOCI method used to parameterize the DIM calculation.
[b]In this work, CCSD(T) computation corrected for BSSE, with the same basis set as for the SOCI method but with 54 electrons explicitly correlated.

is found. Once the equilibrium positions have been obtained, we compute the energy second derivatives with respect to the atomic coordinates to get the Hessian matrix, which is then diagonalized to obtain the vibrational modes of our sample.

The spectrum arising from a given trapping site is generated from these vibrational modes. For a specified temperature, the amplitudes of these harmonic modes are sampled according to the Boltzmann distribution. This provides a set of atomic positions, for which the DIM Hamiltonian of the whole system is computed and diagonalized to get the ground and excited state energies. Note that this method allows us to account for the zero-point energy motion in the very low temperature range. Thus, for each sampled position, we obtain the transition energies from the ground ^1S state to the exited ^1P state. A histogram of the transition energies is thereby constructed to mimic the oscillator strength associated with the excitation spectrum.

III. RESULTS AND DISCUSSION

A. 2D-EE spectra

2D-EE spectra recorded with excitation of the (6s6p) $^1P_1 \leftarrow (6s^2)\ ^1S_0$ transition of Ba atoms isolated in solid Xe are presented in Fig. 1. The colour contour plot and the spectra shown on top were recorded from a sample freshly deposited at 10 K, under conditions of low metal loading, while the 2D-EE scan shown below is the same sample annealed to 60 K and recorded at 10 K. Clearly annealing has a profound effect on the luminescence of this matrix system. The dominant feature in the scan of the freshly deposited sample is a structured band centred at 591.6/557.9 nm (emission/excitation), which exhibits a resolved threefold splitting pattern in excitation as shown by the blue trace on the right. The second most intense feature, centred at 594.7/576.7 nm, does not display any resolved structure. A weaker emission exists at approximately 578 nm, whose excitation intensity is divided into two bands located at 551 and 570 nm. Excitation (vertical) slices taken through the 2D-EE plot at positions X.1 and X.2 are shown overlaid on the absorption trace (T_{dep} = 10 K) in the top panel of Fig. 2.

Annealing the Xe host to 60 K has a dramatic effect on the luminescence of Ba/Xe, as illustrated by the 2D-EE plot shown on the bottom panel in Fig. 1. A comparison with the upper panel reveals that the annealed scan is much more compact, consisting of three well resolved components labeled I–III based on their relative intensities. The excitation spectra extracted at the indicated emission wavelength values X.1, X.2, and X.2b in Fig. 1 are presented in the lower panel of Fig. 2, where they are overlaid onto the annealed absorption profile of Ba/Xe. The excitation profile recorded for the broadest emission band at ~591 nm (X.1) becomes much simpler following annealing. A comparison of the two (X.1) blue traces in Fig. 2 reveals that the spectral location of the threefold split band is unchanged. However, for the annealed sample, the red band located 576.7 nm and a broad blue wing extending to 530 nm have been completely removed leaving a much narrower band. Both wing features are, therefore, attributed to thermally unstable sites of isolation for Ba in solid Xe. The thermally stable threefold split (band I) is a manifestation of the dynamic Jahn-Teller effect[26] and arises from the isolation of Ba in a highly symmetric site within the Xe lattice. The Jahn-Teller (JT) band directly matches the dominant absorption feature but the three peaks are much better resolved in excitation, occurring at 553.9, 557.9, and 562.1 nm. In all cases, the excitation scans recorded in the present study

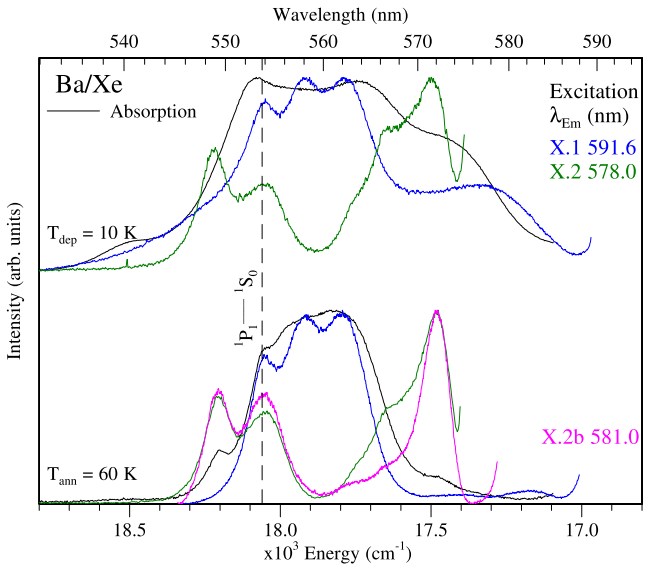

FIG. 2. A summary of the absorption (gray) and excitation (coloured) spectra recorded for Ba/Xe illustrating the effects of sample annealing to 60 K. The excitation spectra were extracted from the 2D-EE scans shown in Fig. 1 by taking vertical slices denoted as X*n*. Most conspicuous in this figure is the removal of broad features to the red of the thermally stable bands and, to a lesser extent, the features to the blue.

provide higher quality data for band shape analysis than the parent absorption profiles. This arises as they are much better resolved than the strongly overlapped absorptions as is clearly evident in the lower panel of Fig. 2. Accordingly, band shape analysis will only be conducted on the excitation scans.

The effect of annealing is less pronounced for the excitation spectra recorded monitoring the 578 nm emission band. As mentioned, this emission displays two regions of intensity in excitation (X.2)—labeled II and III in Fig. 1. Band II is characterised by a dominant component at 572 nm that extends to higher energy with less intense peaks observed at 563.4 and 566.4 nm. Band III comprises a well resolved doublet with peaks at 549.3 and 554 nm. In contrast to the characteristic threefold JT feature, this excitation profile is more challenging to interpret. The observation of five components, two of which are only partly resolved, suggests that two distinct Ba trapping sites contribute to the spectrum. This would occur if the emission bands from each site spectrally coincide. As a test, an excitation scan was obtained by taking a slice (X.2b) through the red wing of the emission at ~581 nm. The resulting spectrum, which is shown by the pink trace in Fig. 2, exhibits a clear connection between the doublet (band III) at 549.3 and 554 nm and the dominant component (band II) at 572 nm. Accordingly, these asymmetric (2 + 1) peaks are attributed to the same site of isolation for Ba. A slice (X.2) taken through the blue side of this emission band (green trace in Fig. 2) accentuates the partly resolved peaks at 563.4 and 566.4 nm, suggesting that these originate from a different, distinct matrix site.

Thus, it appears that three thermally stable sites of isolation exist for Ba/Xe. The dominant site corresponds to a well-defined JT threefold split band and is labeled the "blue" site of isolation. The secondary site displays an asymmetric 2 + 1 splitting, consisting of a pair of bands at higher energy and a single band at lower energy. This feature is referred to as the "violet" site of isolation—as its highest energy component at 549.3 nm is the most blue-shifted of all the absorption peaks. The minor "green" site consists of weak, partially resolved peaks which overlap the lower energy component (band II) of the "violet" site in excitation. The excitation peaks presented in Fig. 6(b) of Fairbank and co-workers' study,[1] match those shown in Fig. 2 except the complete excitation profile of the 572 nm band was not recorded in the earlier work. The reason is that this emission band has a small Stokes shift as is evident in Fig. 1 by the very close proximity of feature II to the excitation diagonal. One other difference with the earlier work is the report of an emission band at 619 nm, which was never observed in the samples prepared in the present study. It is possibly a thermally unstable feature that can be removed with annealing. Other than these two differences, there is good agreement between the earlier and current excitation results. The spectral and dynamical characteristics of the luminescence recorded for each of the three identified sites will now be presented in turn.

B. Blue site

Emission and excitation spectra recorded for the blue site of isolation are presented in the upper panel of Fig. 3. The excitation scan is characterised by a resolved threefold splitting pattern[27,28] centred at 557.8 nm, exhibiting a matrix red-shift of −133 cm^{-1} from the position of the $^1P_1$–$^1S_0$ transition in the gas phase. Photoexcitation of the central component of the JT band produces intense emission centred at 591.6 nm, corresponding to a horizontal slice through the 2D-EE plot shown at M.1 in Fig. 1. A relatively large Stokes shift of 1018 cm^{-1} is extracted from the centre of the excitation and emission bands. A band shape analysis for the excitation profile required the use of three Gaussian curves, each having linewidths (fwhm) of 144 cm^{-1}, to adequately fit the recorded trace. Full details of the fits done on the excitation profiles are presented in Table II. By contrast, fitting the emission band required only a single Gaussian function (fit not shown), characterised by a bandwidth of 311 cm^{-1}.

The temporal characteristics of the blue site emission were investigated with pulsed laser excitation and iCCD detection

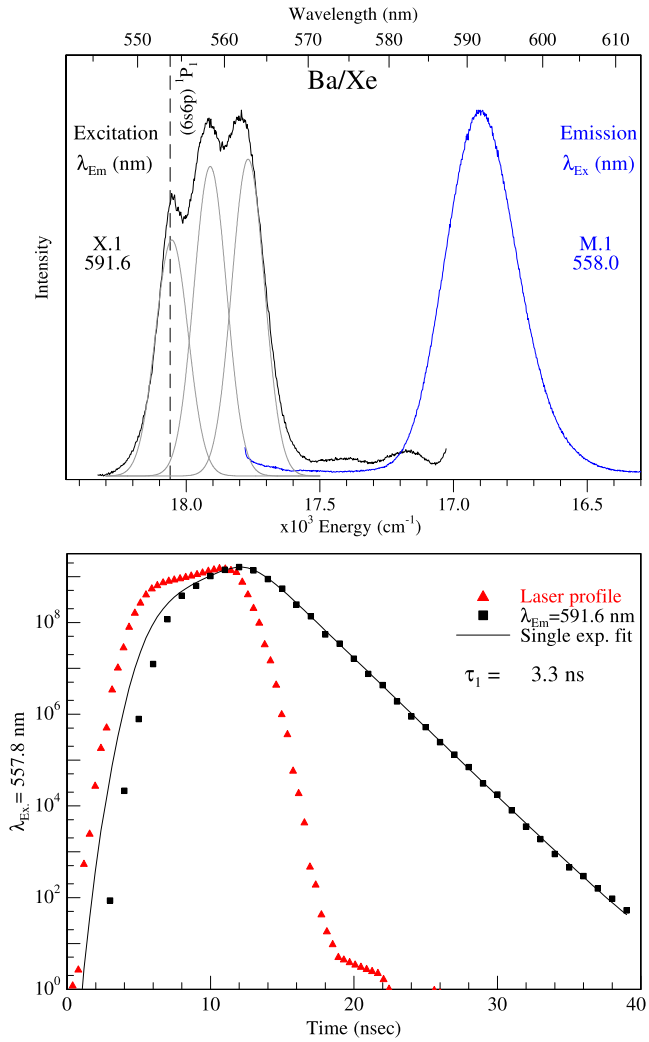

FIG. 3. Luminescence spectra recorded for the blue site of isolation for annealed Ba/Xe. The lack of mirror symmetry in the excitation (X_1) and emission (M_1) profiles is clearly evident as the former exhibits threefold splitting while the emission band is featureless. An emission decay profile recorded at 591.6 nm for the blue site, produced by site-selective laser excitation at 557.8 nm, is shown by the black squares in the lower panel. An excited state lifetime of 3.3 ns was obtained at 10 K by fitting with a single exponential trial function (shown by the solid black line), which included a re-convolution with the time profile of the Nd:YAG laser shown by the red triangles.

TABLE II. Characteristics of the bands extracted for the sites of isolation of Ba atoms in Xe as obtained in Gaussian fits of the excitation spectra recorded for the $(6s6p)\,^1P_1 \leftarrow (6s^2)\,^1S_0$ transition. The fit of the blue site bands is shown in Fig. 3 while those of the violet and green sites are shown in Figs. 5 and 7, respectively. Due to the spectral overlap and the weakness of the green site features, the accuracy of the parameters extracted for this site is considerably less. The column Δν provides the splitting between the three component bands of the three thermally stable sites. The lower portion of the table gives the band positions, widths, and splittings generated in the spectral simulations for the three specified sites.

Site	Band	λ (nm)	ν (cm^{-1})	Δν (cm^{-1})	Relative intensity	fwhm (cm^{-1})
	1	549.2	18 209		0.511	114
Violet	2	553.9	18 054	155	0.467	136
	3	572.2	17 476	578	0.974	132
	1	554.0	18 051		0.645	144
Blue	2	557.8	17 928	123	0.845	144
	3	561.9	17 797	131	0.866	144
	1	563.8	17 737		0.180	97
Green	2	566.2	17 660	77	0.353	84
	3	568.5	17 590	70	0.388	97
	1	544.3	18 372		1.0	72
5V-D_{3h}	2	547.4	18 268	104	1.0	83
	3	563.0	17 763	505	1.0	88
	1	554.4	18 036		1.0	87
TV-T_d	2	557.5	17 936	100	1.0	86
	3	560.3	17 848	88	1.0	103
	1	555.8	17 992		1.0	67
HV-O_h	2	557.7	17 930	38	1.0	56
	3	559.7	17 868	38	1.0	76

as described in Sec. II A. An emission decay profile recorded at 10 K with low intensity dye laser excitation is presented on a semi-log plot in the lower panel of Fig. 3. A decay time of 3.3 ns is obtained by fitting with a single exponential function, which includes a re-convolution with the temporal profile of the Q-switched Nd:YAG laser (red triangles) pulse. This value is considerably shorter than the 8.4 ns radiative lifetime of the excited $6p\,^1P_1$ state for an isolated Ba atom in the gas phase. To further probe the dynamical characteristics of the blue site, the temperature dependence of the emission was investigated up to 36 K to assess competition of non-radiative components with the fluorescence. The left panel in Fig. 4 indicates that the emission band rapidly loses intensity and becomes slightly red-shifted with increasing sample temperature. The panel on the right presents the corresponding temporal behavior. It is evident that the emission decay curves recorded for the blue site exhibit shortening even in the small temperature range, 10–17 K. The extracted emission decay times are shown as a function of temperature in the inset of Fig. 4, where it is clear that a pronounced shortening of the observed lifetimes (τ_{obs}) occurs immediately with raising the temperature from its base value of 9.8 K. This behavior indicates the existence of a non-radiative relaxation pathway, which competes with the $^1P_1$–$^1S_0$ transition for atomic barium in this site of isolation. Thus, even at 10 K, the radiative lifetime has not been identified for the blue site emission. Scans recorded out to 850 nm did not reveal the presence of any additional emission bands at elevated temperatures. Particular attention was given to the region of the ^3P states of atomic barium, which occur in the gas phase from 740 to 815 nm.

C. Violet site

Emission and excitation spectra recorded for the violet site of isolation are presented in Fig. 5. The excitation features of this site, shown on the left in the figure, occur to the blue and to the red of the gas phase $^1P_1$–$^1S_0$ line. A matrix red-shift of 578 cm^{-1} is evaluated for the dominant excitation band at 572 nm. The lower energy peak of the pair at 553.9 nm overlaps

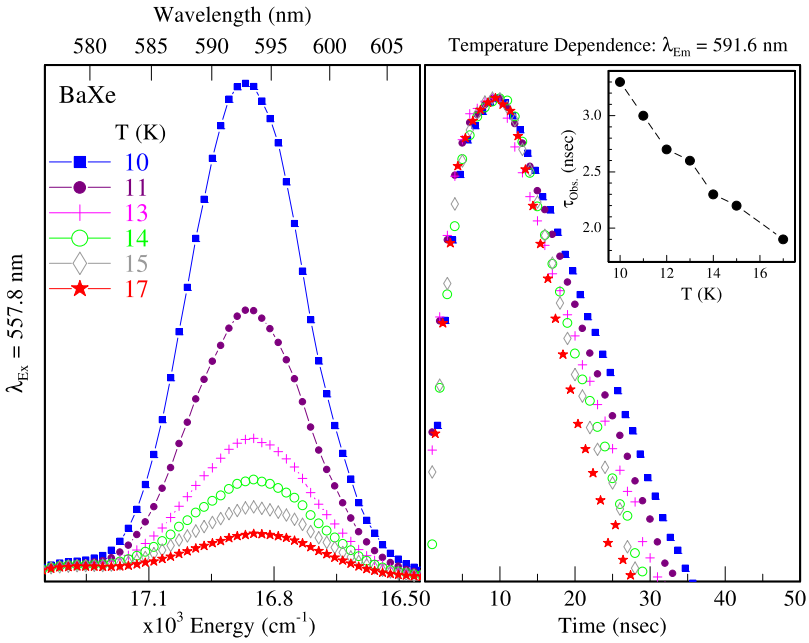

FIG. 4. The left panel shows the temperature dependence of the Ba/Xe blue site emission band at 591.6 nm. A small but progressive red-shift of the band centre occurs in conjunction with a pronounced decrease in the band intensity, as the sample temperature increases from 10 to 17 K. The right panel presents the temperature dependence of the corresponding emission decay curves. The inset shows the extracted decay times as a function of the sample temperature revealing the shortening of the observed lifetime as soon as the temperature is increased above the minimum value of 10 K.

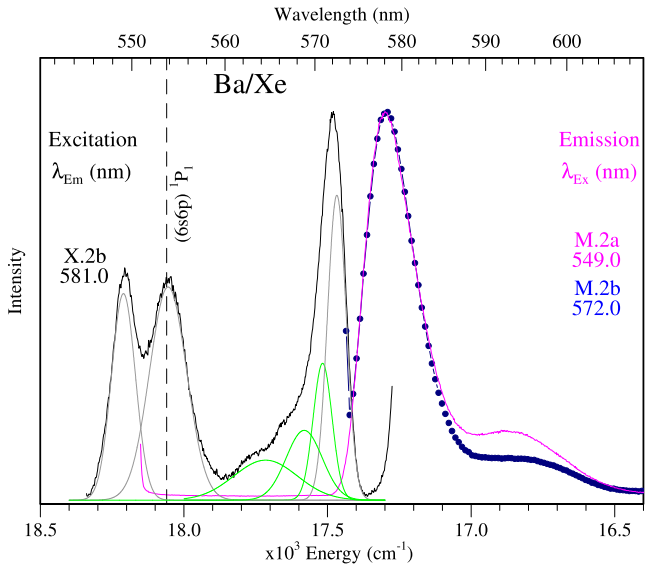

FIG. 5. Emission (coloured) and excitation (black) spectra recorded at 10 K for the violet site of isolation of Ba in solid Xe. The excitation profile was obtained by monitoring the emission at 581 nm. This was done to minimise the contribution of the green site, which emits in-close proximity at 577.1 nm. However, due to the overlap of the two emission bands some of the green site still persists as shown by the three green traces obtained from a line shape fit of the excitation profile. The excitation scan of this violet site clearly differs from that of the blue site, exhibiting a 2 + 1 asymmetric splitting pattern. The Stokes shift is also considerably smaller than for the blue site.

the gas phase position displaying a very small red-shift of 6 cm^{-1}, whereas the remaining doublet peak at 549.3 nm is blue-shifted by +145 cm^{-1}.

A line shape analysis of the excitation spectrum shown in Fig. 5 required the use of a total of six Gaussian curves to fit the scan profile. Three of these (shown in green) account for the minor amount of the green site features present due to the spectral overlap between the violet and green site emission bands. Two of the green site bands are partially resolved features located at 566.4 and 563 nm, while the other is not evident in the recorded profile. The line shape fit shown in Fig. 5 reveals that these features make up the blue wing of the lowest energy band of the violet site, which enhances the intensity of the singlet compared with the doublet bands. Each peak of the violet site 2 + 1 structure is fitted with a single Gaussian, shown by the gray traces and the extracted values are collected in Table II. The highest energy component of both the doublet and the lower energy singlet band is relatively narrow, displaying bandwidths (fwhm) of 98 and 91 cm^{-1}, respectively. The remaining doublet component is broader, exhibiting a fwhm of 152 cm^{-1}. However, this value may be skewed due to the spectral overlap with the highest energy component of the blue site JT band. Photoexcitation into any of the three absorption peaks produces emission at 578.1 nm characterised by a bandwidth of 213 cm^{-1} and a slightly asymmetric band shape which tails to lower energy. The emission scans shown in Fig. 5 correspond to the horizontal slices taken at the indicated excitation values, M.2a and M.2b in Fig. 1. The Stokes shifts evaluated from each excitation peak (high to low energy) are 907, 756, and 184 cm^{-1}. An emission decay profile recorded at 10 K for the violet site 578.1 nm band, produced with laser excitation at 549.1 nm, yielded an excited state lifetime of 4.3 ns by fitting with a single exponential trial function. Decay profiles recorded with excitation of the lower energy violet site bands were similar and yielded the same lifetime values.

Spectral and temporal scans recorded for the 578.1 nm emission band at elevated temperatures are presented in the left and right panels of Fig. 6, respectively. As shown, the emission loses intensity and becomes red-shifted over the 10–36 K temperature range investigated. Examining the right panel of this plot reveals that the corresponding decay profiles are unaffected by the sample temperature below 24 K. As shown in the inset of Fig. 6, where the extracted lifetimes are presented, the radiative lifetime has been measured to be 4.3 ns for the violet site emission. At 24 K, a noticeable shortening of the observed decay time occurs indicating that a non-radiative relaxation

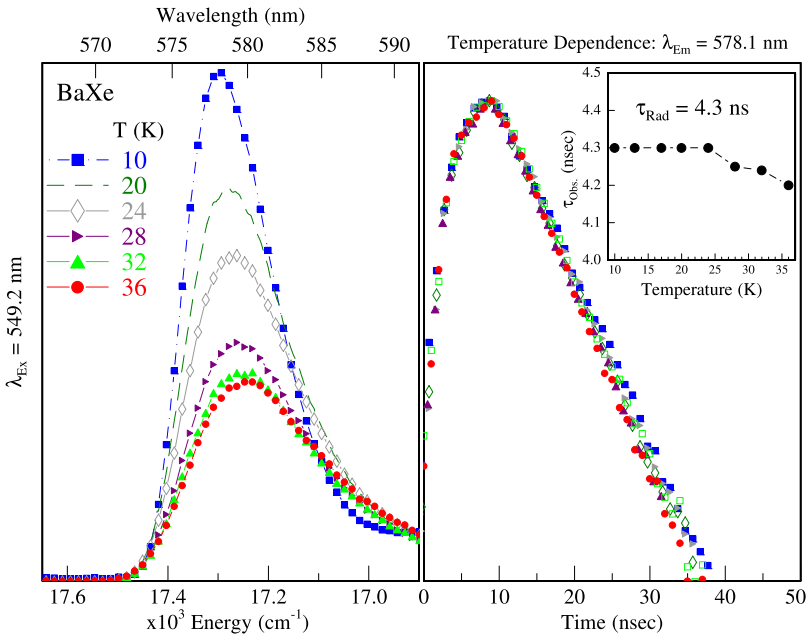

FIG. 6. The left panel shows the temperature dependence of the Ba/Xe violet site emission band at 578.1 nm produced with site-selective laser excitation at 549.2 nm. A progressive red-shift of the band centre occurs in conjunction with a significant decrease in the band intensity, as the sample temperature increases from 10 to 36 K. The right panel presents the temperature dependence of the corresponding decay curves which were obtained with time-gated detection and pulsed laser excitation. The inset shows the variation of the extracted decay times revealing that there is no change in the 4.3 ns value extracted at 10 K until approximately 25 K when it begins to shorten.

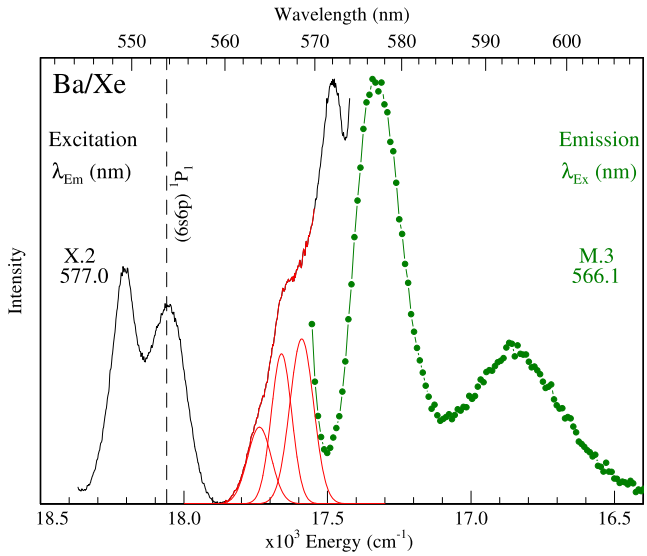

FIG. 7. Emission (green) and excitation (black/red) spectra recorded at 10 K for the green site of isolation of Ba in solid Xe with site-selective laser excitation at 566.1 nm. The excitation profile was obtained by monitoring the emission at 577 nm. The portion of the excitation trace highlighted in red corresponds to the features which are associated with the green site.

pathway becomes active and competes with the fluorescence above this temperature.

D. Green site

Figure 7 presents the spectral characteristics of the minor, green site luminescence of Ba/Xe. It is evident that this excitation spectrum, shown on the left, is dominated by the more intense features of the violet site. For clarity, the excitation features associated with the green site are highlighted there in red as the three fitted Gaussian curves. The parameters of this fit are provided in Table II. A matrix red-shift of –405 cm^{-1} is determined from the partially resolved band at 566.4 nm. Photoexcitation at 566 nm produces an emission band at 577.1 nm showing a bandwidth of 202 cm^{-1}, corresponding to a horizontal slice through the 2D-EE plot shown at M.3 in Fig. 1. Thus, this emission is shown to be distinct from that of the violet site, despite both bands occurring in the same spectral region. The weaker emission band centered at 592 nm arises due to the overlap with the blue site absorption [see Fig. 3(a)].

A decay profile of the green site emission at 577.1 nm was recorded with laser excitation at 568.9 nm, and a single exponential function with a lifetime of 4.0 ns provided a satisfactory fit. This value is slightly shorter than that recorded for the violet site. The temperature dependences observed in the spectral and temporal scans are presented in Fig. 8. Examination of this figure illustrates that although the emission intensity decreases, the temporal profile does not change until above 13 K. Thus, as indicated in the inset of Fig. 8, the radiative lifetime has been identified as 4 ns—the value recorded at 10 K. In contrast to the violet site, the recorded lifetime of this band becomes gradually shorter at temperatures above 13 K. For instance, a value of 3.0 ns is observed at 28 K, indicating the existence of a non-radiative process, which competes effectively with the fluorescence of the green site. The activation temperature of this process is slightly higher than that of the blue site, as can be gleaned from a comparison of the insets of Figs. 4 and 8.

E. Temperature dependence

Time-integrated spectral scans and time-resolved decay profiles were recorded for each site-specific emission band over a range of temperatures. This was done to investigate the non-radiative relaxation pathways competing with the radiative (6s6p) $^1P_1 \rightarrow {}^1S_0$ ($6s^2$) fluorescence of Ba at a given site. Most Ba/RG emission bands show a decrease in the integrated area at higher temperatures. However, absorption and emission scans recorded back at 10 K indicate that bleaching and/or site interconversion results in a loss of signal—even with low intensity laser or lamp irradiation. Therefore, two effects can

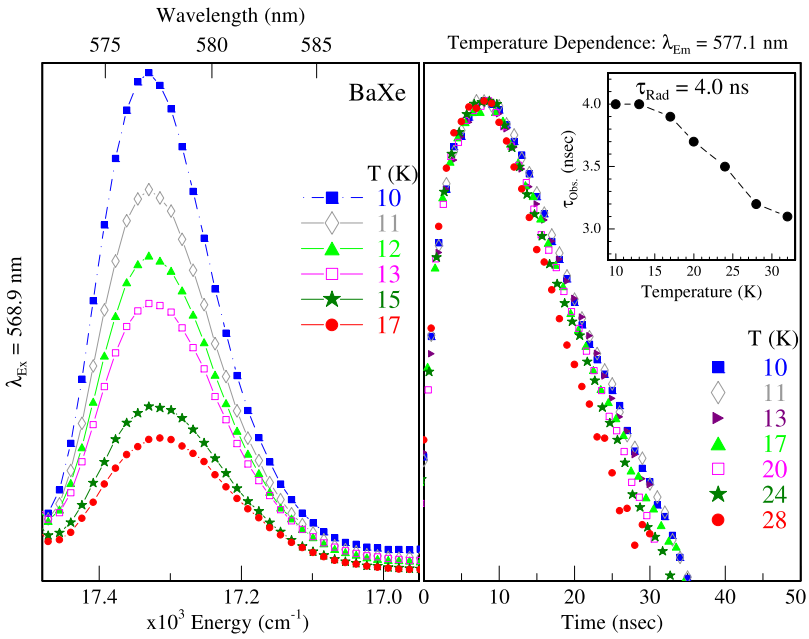

FIG. 8. The left panel shows the temperature dependence of the Ba/Xe green site emission band at 577.1 nm. A slight red-shift of the band centre occurs in conjunction with a decrease in the band intensity, as the sample temperature increases from 10 to 17 K. The right panel presents the temperature dependence of the decay curves recorded over a wider range from 10 to 28 K. The decay profile recorded at 10 K for the emission band at 577.1 nm yielded an excited state lifetime of 4.0 ns when fit with a single exponential trial function. This value remains unchanged until approximately 13 K when it begins to shorten rapidly.

lead to a decrease in the integrated area of a band over a given temperature range. However, the time-resolved scans provide a distinction, as bleaching and site interconversion should not affect the decay time of an emission band.

Of the three Ba/RG systems studied,[29] the decay profiles and emission bands of Ba/Xe displayed the greatest temperature dependence. It was noted in a comparison of the effective-field corrected matrix lifetimes with the gas phase λ^3 extrapolation presented in Ref. 29 that the Ba/Xe blue site lifetime is the only value shorter than the gas phase value. Even in the small 10–17 K range shown in Fig. 4, the observed lifetime of the blue site shortens dramatically from 3.3 to 1.8 ns. Therefore, the radiative lifetime of this site of isolation was not obtained at 9.8 K—the lowest temperature achievable in the current experimental set-up. The integrated area of the emission is also vastly reduced and cannot be accounted for by bleaching or site interconversion alone. A similar effect was observed for the green site of isolation, however, the lifetime (4.0 ns) obtained at 10 K only began to shorten at temperatures above 13 K. The lifetime of the violet site in Xe was observed as 4.3 ns at 10 K and did not shorten until temperatures of 24 K or greater were reached. Thus, the true radiative lifetimes were measured for the green and violet sites in Xe but not for the blue site.

Figure 9 presents a comparison of the Ba/Xe excitation scans (X.1 and X.2 of Fig. 1) recorded at 10 and 35 K. A striking difference between the two panels is the absence of the blue and green site excitation bands at 35 K, an effect occurring because the intensities of these emission bands have all but vanished at this temperature. However, the blue site profile at 35 K can be obtained from absorption measurements, as shown by the black trace in the top panel of Fig. 9. By contrast, the violet site emission band at 578.1 nm still exhibits significant intensity at 35 K, although the maximum has red-shifted to 580.1 nm. The corresponding excitation spectrum recorded at 35 K is simpler than its 10 K counterpart as it is free of overlap with the green site, exhibiting the clearest 2 + 1 structure. From a line shape analysis conducted on the violet site 35 K excitation scan, it emerges that the corresponding peak widths are more equal but considerably broader than for the 10 K scan, displaying bandwidths of 143, 168 (doublet), and 146 cm^{-1} (singlet). It is also noteworthy that the position of the lower energy doublet band shifts further to the red at 35 K than the two other bands in the 2 + 1 asymmetric feature.

From the strong temperature dependence identified in the observed Ba/Xe emission, it is clear that the ^1P state fluorescence of atomic Ba isolated in solid Xe is being quenched by a non-radiative relaxation process. A qualitative explanation for this effect emerges from the excited state potential energy curves (PEC) calculated for Ba·Xe in the present study with the MRCI method outlined in Sec. II B. The excited states of relevance to the relaxation of ^1P state atomic barium are shown in Fig. 10. Of particular importance to this process is the crossing that occurs between the bound $^1\Pi$ state and the repulsive $^3\Sigma$ state correlating with the ^1P and ^3P atomic asymptotes, respectively. As shown, the $^3\Sigma$ curve crosses slightly above the bound region of the $^1\Pi$ giving rise to site-specific and temperature dependent $^1P \rightarrow {}^3P$ intersystem crossing (ISC). It is this initial crossing which leads to fluorescence quenching that dominates all Ba/Xe sites at elevated temperatures. The recent PECs for Ba–Xe, calculated by Abdessalem[24] and co-workers, including configuration interaction but using pseudopotentials, have obtained similar results which demonstrate also a crossing between these two curves.

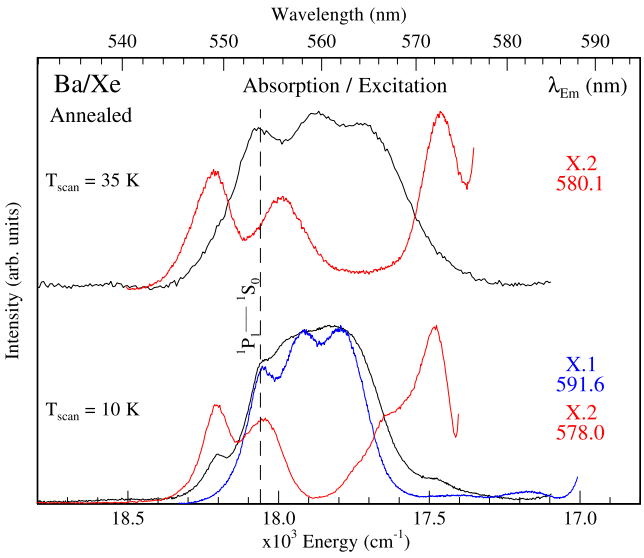

FIG. 9. A comparison of the absorption (black) and excitation (coloured) bands of Ba/Xe recorded at 10 K (lower panel) versus 35 K. The blue site JT band is notably absent at 35 K in excitation as its emission intensity has all but vanished at this temperature. Contrasting this, the violet site has significant intensity at 35 K and its characteristic 2 + 1 splitting pattern is still evident but the lower energy component of the "2" bands moves to a more central position. All the excitation/absorption bands are significantly broader at 35 K than at 10 K.

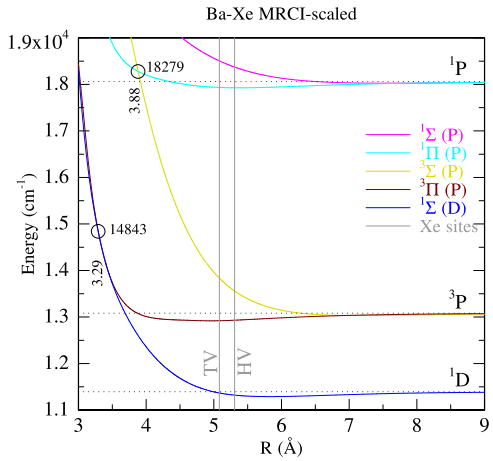

FIG. 10. Excited state potential energy curves calculated for diatomic Ba·Xe with the MRCI method showing the molecular $^1\Pi(6p^1P)$ and $^1\Sigma(6p\,^1P)$ states used in the simulations of the absorption (excitation) spectroscopy of the $^1P_1 \leftarrow {}^1S_0$ transition of atomic barium in solid xenon. The ground $^1\Sigma(6s\,^1S)$ state used is not shown for presentational reasons to highlight the states relevant to the luminescence and non-radiative relaxation observed for the excited ^1P state metal atom. State crossings of significance to the latter process are highlighted by the circles shown in the plot. The associated numerical values are the inter-nuclear distances and energies (Å and cm^{-1} respectively) for the identified curve crossings.

The current MRCI PEC's also provides a possible explanation for the lack of ^{3}P emission observed in the present Ba/Xe matrix work as a consequence of ISC from the ^{1}P state. By contrast, the classic gas phase, laser pump-probe investigation conducted by Breckenridge and Merrow[30] of the collisional deactivation of Ba (6s6p) $^1P_1$ by the rare gases (He–Xe), showed that of the seven possible lower lying accessible states of Ba ($^3P_{J=2,1,0}$, $^1D_2$, and $^3D_{J=3,2,1}$), the $^3P_2$ state is exclusively produced. As shown in Fig. 10, the bound $^3\Pi$ state (with the ^{3}P asymptote) is crossed by the repulsive $^1\Sigma$ state correlating with the ^{1}D state, but this crossing occurs nearly two thousand wavenumbers above the ^{3}P state. In the gas phase, this crossing is never explored because of the strongly dissociative nature of the $^3\Pi$ state at this short distance (~3.3 Å). In the matrix, the ^{3}P state Ba atom resulting from ISC is produced with large kinetic energy (roughly equal to the energy difference between the ^{1}P and ^{3}P atomic states) but is trapped in its site of isolation. This highly energised Ba atom can come close enough to another Xe atom in its first surrounding sphere so that the crossing is accessible. Moreover, as this energy is much larger than the thermal energy, several lattice vibrations are necessary to dissipate it through the matrix so the ^{3}P state barium atom will remain energised for many vibrational periods resulting in multiple crossing events. It can thus come close enough to the crossing region to allow for some coupling to occur. As a result, $^3P \rightarrow {}^1D$ state relaxation occurs in the solid state environment[31] of the Ba/Xe matrix producing the ^{1}D state. Emission of this state to the ground state is outside the spectral range of our[29] detection system which explains the lack of atomic emission at elevated temperatures when the ^{1}P state fluorescence is quenched.

F. Model trapping sites

To investigate the isolation of barium atoms in xenon, we considered two varieties of trapping sites. The first variety is obtained by removing a selected number of atoms from the perfect lattice of the Xe crystal. Previous experience suggests that the single vacancy SV(O_h), tetra-vacancy TV(T_d), and hexa-vacancy HV(O_h) trapping sites are possible candidates for spectral bands that exhibit well defined three-fold Jahn-Teller splitting.[7,16] Inspection of the equilibrium bond length of the Ba·Xe pair indicates, as suggested in Ref. 2, that the SV site is too small to accommodate the large Ba atom in its ground state. The TV site is a natural candidate for the blue site observed experimentally, while the HV site produces a rather small Jahn-Teller splitting and is probably unstable against annealing. It might, therefore, be a candidate for the green site which remains, but in quite small amounts, after annealing. Other *fcc* crystalline sites, such as the trigonal planar, trivacancy (D_{3h}), and the square-pyramid, five-vacancy (C_{4V}) sites were considered here to analyze the strong 2 + 1 violet feature. While the simulated bands for both sites exhibited pronounced asymmetric splitting of the $^1P \leftarrow {}^1S$ absorption profile, the energies of the doublet/singlet features were found to be the reverse of what is observed experimentally. Thus, both these sites present the doublet at lower energy relative to the singlet but as shown in Fig. 5, the opposite order is observed for the recorded excitation band.

The second variety of sites is obtained from grain boundaries. In the case of alkali atoms, some of these trapping sites reproduce quite well the observed absorption spectrum. However, they are usually less stable than the crystalline trapping sites because the guest atoms can migrate more easily along the grain boundary. In the case of the alkali metal atoms, such a migration favors the formation of alkali dimers and larger metal clusters, which have a very large binding energy compared with the alkali-rare gas interaction. In the case of an alkaline earth metal atom, however, the energy balance is not so favorable and we may expect the boundary site to be more stable. The present experimental results have shown that the violet site is characterized by a low energy singlet band, well separated from a higher energy doublet. We have, therefore, looked for elongated uniaxial trapping sites and have found that a five atom vacancy (5V) site with D_{3h} symmetry can be formed at a grain boundary resulting from stacking fault. This trapping site is illustrated in the top panel of Fig. 11, where it can be compared with the tetra-vacancy of the *fcc* lattice. The boundary plane of the 5V(D_{3h}) site coincides with the 111 plane of both grains with the result that there is no lattice mismatch at the interface of the two grains. The existence of a similar 5V(D_{3h}) site inside an *hcp* crystallite is possible and cannot be definitely ruled out. However, the amount of *hcp* phase is limited[4] and it is likely to disappear by annealing while twins and stacking faults were observed without the formation of the *hcp* phase. Consequently, this "defect" site is quite stable under annealing. There are of course an infinite number of possible grain boundaries, but most of them are energetically less favorable. We cannot exclude that other grain boundary geometries might give a similar site, though we did not find any. The radial distribution function (RDF) depicted at the bottom of Fig. 11 shows, in a complementary way, the geometric arrangement of the Xe atoms around the Ba impurity. We see clearly in this figure that the first neighbouring shell of the TV T_d site, with 12 Xe atoms, turns into two shells in the case of the 5V D_{3h} site, the closest shell with 3 Xe atoms, the next nearest one containing 12 Xe atoms.

Once a trapping site has been chosen, the matrix sample is relaxed to obtain the corresponding equilibrium geometry and a spectrum is generated as described in Sec. II B. Simulated excitation spectra for the TV and 5V sites are depicted in Fig. 12, where they are compared with the recorded spectra. The TV spectrum shows an obvious three-fold Jahn-Teller splitting whose magnitude matches that of the experimentally observed band for the blue site. The positions of the simulated and experimental spectra also match up quite well. The simulated emission is centered around 593.2 nm, also in quite good agreement with the experiment. The other crystalline trapping sites investigated here do not produce any spectrum comparable to the experimental ones.

The simulated excitation spectrum for the 5V(D_{3h}) site, shown by the red trace in the bottom of Fig. 12, clearly exhibits the features recorded for the violet site with a well-defined double peak on the high energy side and a single peak on the low energy side. The simulated emission is centered around 568 nm, i.e., slightly red shifted with respect to the reddest absorption peak. Like the TV spectrum, it is also reasonably well located with respect to the experimental spectrum.

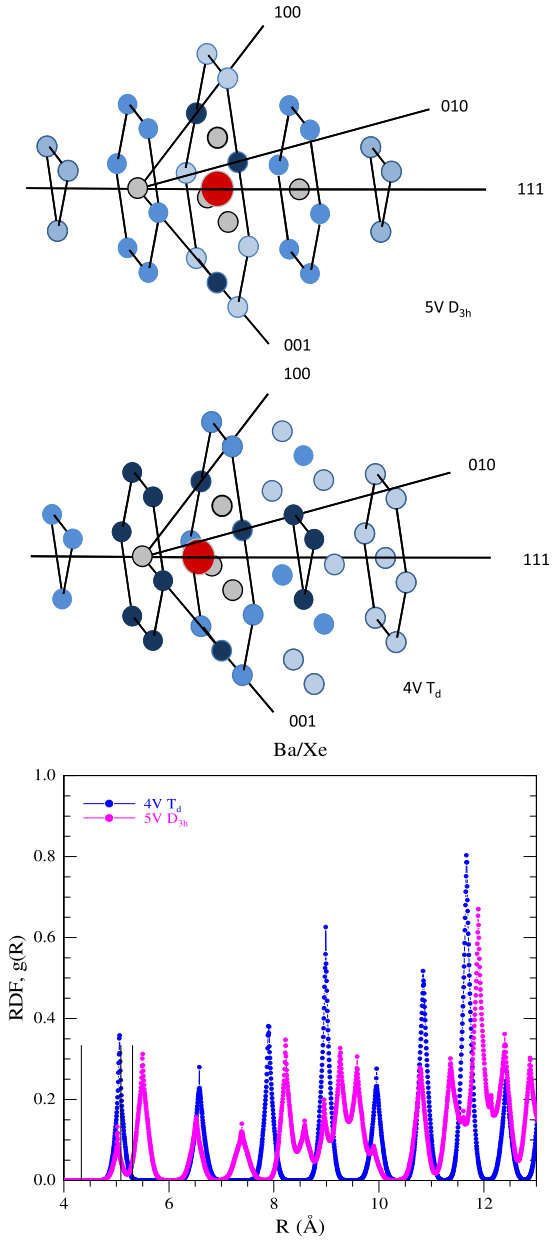

FIG. 11. Comparisons of the structures of the 5V D_{3h} and 4V T_d trapping sites used in the Ba/Xe spectral simulations. In the upper two panels, the lattice structure in the vicinity of the vacancies is represented, while in the bottom, the radial distributions calculated for the relaxed structures of the two sites are presented together. For both sites, the host atoms on 5 planes perpendicular to the (111) direction are shown around the Ba impurity, which is depicted in red. The matrix atoms in the first and second coordination shells around Ba are dark- and medium-blue coloured, respectively. The gray atoms correspond to the vacancies. The three first planes on the left are identical for both sites. The middle plane in the 5V D_{3h} site is the grain boundary plane and a symmetry plane for the twin grains. The two other planes on the right are different. The radial distribution functions (RDF) computed for the relaxed TV (T_d) site and for the 5V(D_{3h}) were obtained by sampling the harmonic modes of a Ba·$(Xe)_N$ cluster at a temperature of 10 K. The equilibrium structure and modes were determined with the CCSD(T) potential for the ground state of Ba·Xe (given in the supplementary material) and using Aziz and Slaman's [Mol. Phys. **57**, 825 (1986)] potential for Xe·Xe. The number of Xe atoms in the cluster was N = 600 and N = 815 for the TV and 5V sites, respectively. Shown for comparison, by the vertical black lines, are the tetra- and hexa-vacancy (TV and HV) site sizes calculated from the lattice parameter of pure Xe. It is noteworthy that the nearest host atoms in the guest-occupied TV site and especially the 5V site are slightly closer to the barium atom than in the TV site of the pure Xe lattice. This represents a small contraction of the lattice in the vicinity of the guest atom isolated in the multi-vacancy TV and 5V sites.

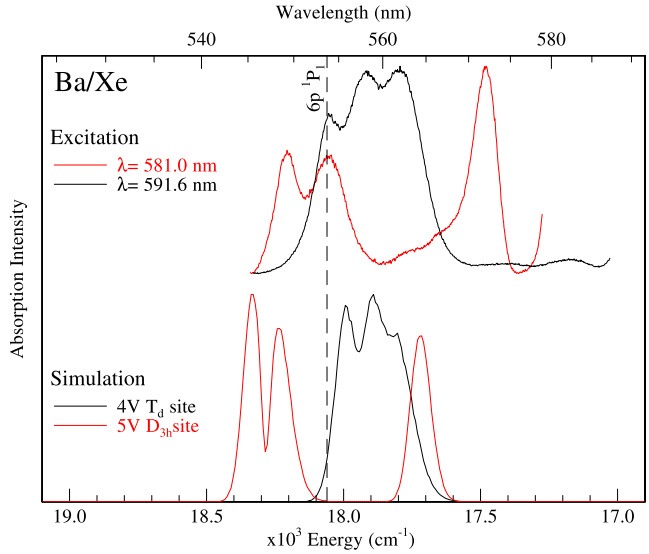

FIG. 12. A comparison of the simulated absorption spectra (lower traces) with the recorded excitation spectra for the two dominant thermally stable sites in the Ba/Xe system. The excitation spectra were recorded at 10 K while the simulated absorptions pertain to the Ba atom isolated in the 4V (T_d) site and the 5V (D_{3h}). The close agreement of the recorded and simulated spectra allows clear attribution of the latter to the violet "2 + 1" site while the former site gives rise to the blue, threefold split Jahn-Teller band.

Regarding the spectral shape of this 5V site in excitation, we recall that Boatz and Fajardo obtained a similar shape for absorption bands simulated for a Na atom trapped in an Ar lattice with 2 or 5 atoms removed. In this earlier work, a cluster,[16] consisting of 105 Ar atoms, was used to model the matrix. Similar to the SV site, we estimate that the double vacancy site is too cramped and unlikely to accommodate the large barium atom. Furthermore, the 5V site reported in Ref. 16 is probably not a cubic lattice as we notice that the radial distribution function (RDF) shown for this site is virtually the same as that shown for the TV site. In the bottom panel of Fig. 11, we compare the RDF's determined in the present work for the 5V(D_{3h}) site and the TV(T_d) site. The RDF's of the TV sites match in the present and the previous study in Ref. 16 but the 5V sites are very different. In the current study, the number of Xe atoms used in the cluster to model the crystal was N = 600 and N = 815 for the TV and 5V sites, respectively. It is likely that in the small cluster of Ar atoms (N = 105) used in Ref. 16 the structure collapsed around the large 5V and in so doing, regenerated the tetravacancy site around the Na atom. The much bigger samples used in the present work ensure that the cluster maintains the original symmetry.

The line shape analyses conducted for the three site-resolved excitation bands are shown in Figs. 3, 5, and 7 for the blue, violet, and green sites, respectively. The results of these fits are collected in Table II, as well as a comparison with the spectral simulations for the TV-T_d, 5V-D_{3h}, and HV-O_h sites. This table presents the splittings between the individual band components ($\Delta\nu$) as well as intensity information (the heights and widths) of each feature. It should be pointed out that the splittings between the components of the green site are roughly equal ($\Delta\nu$ = 70 and 77 cm^{-1}) as found in the blue site (123 and 131 cm^{-1}). This behavior is indicative of

Jahn-Teller splitting for highly symmetric sites as presented in the TV-T_d and HV-O_h sites. In stark contrast, the violet site exhibits very unequal splittings of 155 and 578 cm^{-1} indicative of the presence of another effect. This asymmetric 2 + 1 splitting will be discussed in Sec. III G. It is also evident in Table II that the simulated bands are systematically narrower than the bands recorded in the experiment. This may be due to the limited accuracy of the potentials used in the simulation for the Ba–Xe and Xe–Xe interactions. Nevertheless, the general trends are well reproduced. Moreover, the ratios of the average width from one site to another are comparable in the experiment and simulation. The simulated peak shifts $\mathbf{\Delta\nu}$, which signs the shape of the site, are also quite comparable with their experimental counterparts.

G. Origin of the 2 + 1 splitting

As noted already, the asymmetric 2 + 1 splitting observed in excitation for the violet site in the Ba/Xe system is the first documented instance of this behavior for a matrix-isolated metal atom. By contrast, the threefold splitting on the blue site is typically encountered in matrix spectra. While these situations initially seem quite different, the characteristic band shapes of the 5V D_{3h} and TV T_d spectra can both be understood by considering the relative contributions of a static crystal potential, V, originating from the lattice and its dynamical distortion, W, induced by the vibrations of the lattice atoms. This is best analyzed by considering the mean electric potential experienced by the Ba electrons, a situation that can be described by the spherical harmonics Y_{lm}, whose expansion depends on the trapping site symmetry. Thus the coupling $A_{mm'}$ among the 3 states m of the Ba atom 6s6p(^{1}P) shell is governed by symmetry rules. For the sake of simplicity, and consistent with our DIM calculation, the couplings with the other Ba atom states are neglected here. For some potential U = V or W, A can be expressed as

$$A_{mm'} \propto \int d\Omega Y^*_{lm}(\Omega)\, Y_{lm'}(\Omega)\, U(\Omega) = \sum\nolimits_{\lambda\mu} \int d\Omega Y^*_{lm}(\Omega)\, Y_{lm'}(\Omega)\, U_{\lambda\mu}(\Omega).$$

Using the properties of the spherical harmonics, only the terms $\lambda = 0, 2$ and $m-m'-\mu = 0$ contribute to the sum. The spherical term U_{00} is essentially a global shift of the three energy levels and can be omitted for our purpose. The active terms are thus $U_{2\mu}$ only.

In the absence of dynamical vibration W = 0 and the only contribution to the total potential U is U_{20}. Only A_{00} is non-vanishing and the degeneracy between $m = 0$ and the two other states $m = +1$ or $m = -1$ is lifted. This effect is significant in the case of the 5V D_{3h} site because of the large overlap with the 3 nearest neighbors in the boundary plane, which induces a large U_{20} component. In the absence of vibration, we expect to observe one red-shifted peak with relative amplitude 1 and one blue-shifted peak, with relative amplitude 2. There is no such contribution for the site with T_d symmetry and the static potential does not lift the degeneracy of the TV site. We observe thus one single peak with relative intensity 3. The static interaction alone does not produce any splitting of the band for the T_d site.

When the lattice vibrations are taken into account, the symmetry of the trapping site is broken. The five $U_{2\mu}$ terms are thus active to couple the Ba 6s6p(^{1}P) states and all the $A_{mm'}$ terms are non-vanishing. This additional dynamical coupling removes the remaining degeneracy. The angular momentum projections m are no longer good quantum numbers and the three 6s6p(^{1}P) states mix with each other to produce an electronic cloud distorted according to the instantaneous shape of the cavity. The 5V (D_{3h}) site results in a spectrum consisting of 2 + 1 peaks while the TV (T_d) site produces a series of 3 peaks as observed for several ^{1}P and ^{2}P state metal atoms in rare gas matrices. The separation of the peaks and their broadening depends merely on the actual amplitude of the potential W induced by the lattice vibration. It is specific to the guest-host interaction and to the size of the trapping site.

IV. CONCLUSIONS

Ba/Xe emission spectra recorded to 850 nm presented only ^{1}P state fluorescence with no signal detected from any of the ^{3}P states. These occur in the gas phase[32] between 739.9 and 815.3 nm. Excitation spectra extracted from 2-dimensional excitation-emission scans of the total ^{1}P fluorescence, recorded for annealed matrix-isolated barium samples, have revealed that two dominant thermally stable sites are occupied by atomic barium in xenon. In addition to the conventional three-fold split (Jahn-Teller) excitation band, labeled the blue site, the present study provides clear experimental evidence of an elongated trapping site characterized by a band consisting of a blue-shifted double peak and a red-shifted single peak. This "2 + 1" site has never been identified for other metals in rare gas matrices but was observed in the recent Ba/Xe study of Ref. 1. On the basis of the agreement found between molecular dynamics simulations and the recorded site-selected excitation spectra, we can assign the blue band to the crystalline 4-atom vacancy with tetrahedral symmetry (T_d) while the violet band arises from a 5-atom vacancy with trigonal bipyramidal symmetry (D_{3h}). The 5-atom vacancy site recreates the unusual 2 + 1 band profile very convincingly and even though it exists at a grain boundary, it is remarkably stable against annealing.

The spectral and temporal characteristics of all the excitation bands (violet, blue, and green) were examined in a temperature dependent study, revealing a strong influence of the site occupied by the barium atom. Emission scans recorded at elevated temperatures exhibited reduced intensities for the green site but those recorded for the dominant blue site band were completely quenched. By contrast, emission recorded for the violet site was found to be independent of temperature up to 25 K. These temperature dependences were also observed clearly in the recorded temporal profiles with evidence of a non-radiative process competing for the luminescence of the blue site even at 9.8 K. For the blue, green, and violet sites in Xe, the activation temperatures are <10 K, >13 K, and >24 K, respectively. The increased efficiency of the ^{1}P to ^{3}P transition in the blue site is clearly related to the smaller

size of this vacancy. When isolated in the 5V(D_{3h}) site, the excited ^{1}P state behavior of the Ba atom is evidently less sensitive to non-radiative relaxation processes than the other more crystalline sites. The absence of emission from the ^3P_J states at elevated temperatures indicates that further relaxation (either radiative or non-radiative) occurs in the matrix to one of the lower lying potential energy curves which correlate with the ^{1}D and ^{3}D atomic asymptotes. If this secondary intersystem crossing occurs, it is expected that long-lived emission would be observed from the ^{3}D state of Ba. The emission of this meta-stable level occurs at 1107 nm, in the near-IR spectral region, which is outside the range of our current detection system. Multi-reference configuration interaction calculations of the excited state potential energy curves of diatomic Ba-Xe have provided initial insights into the non-radiative intersystem crossing observed in the Ba/Xe samples. Determining the trajectories of the excited $^1P_1$ state barium atoms with the current Ba-Xe potentials should provide a means to fully understand the role the site of isolation plays in this regard.

The spectral simulations conducted on the two dominant thermally stable sites for Ba/Xe have provided new insights into the solid state effects producing such different band shapes for the blue and violet sites. The 2 + 1 structure of the violet site band is attributed to an initial static (crystal field) splitting arising from the distinct axial and equatorial orbital orientations in the trigonal bipyramidal symmetry (D_{3h}), 5-atom vacancy. This is then followed by a dynamic Jahn-Teller vibrational interaction which removes the degeneracy of the equatorial pair. For the blue site, the higher tetrahedral symmetry (T_d) of the tetra-vacancy produces no static splitting and only the dynamic effect of the lattice vibrations removes the degeneracy of the three equivalent p-orbital orientations. This distinction of static and dynamic effects is very clearly illustrated in excitation spectra recorded for the thermally stable sites in the Ba/Xe matrix-isolation system.

SUPPLEMENTARY MATERIAL

See supplementary material for the excited state potentials calculated for BaXe with the MRCI technique.

ACKNOWLEDGMENTS

This research was in part funded by the John & Pat Hume award at N.U.I.-Maynooth which provided Barry Davis with a Ph.D. studentship.

[1] B. Mong *et al.* (nEXO Collaboration), Phys. Rev. A **91**, 022505 (2015).
[2] B. M. Davis and J. G. McCaffrey, J. Chem. Phys. **144**, 044308 (2016).
[3] J. Visticot, P. de Pujo, J. Mestdagh, A. Lallement, J. Berlande, O. Sublemontier, P. Meynadier, and J. Cuvellier, J. Chem. Phys. **100**, 158 (1994).
[4] Y. Sonnenblick, Z. H. Kalman, and I. T. Steinberger, J. Cryst. Growth **58**, 143 (1982).
[5] E. Knözinger, E. Babka, and D. Hallamasek, J. Phys. Chem. A **105**, 8176 (2001).
[6] A. Schrimpf, G. Sulzer, H.-J. Stöckmann, and H. Ackermann, Z. Phys. B: Condens. Matter **67**, 531 (1987).
[7] E. Jacquet, D. Zanuttini, J. Douady, E. Giglio, and B. Gervais, J. Chem. Phys. **135**, 174503 (2011).
[8] R. Bullough, H. R. Glyde, and J. A. Venables, Phys. Rev. Lett. **17**, 249 (1966).
[9] J. A. Venables, C. A. English, K. F. Niebel, and G. J. Tatlock, J. Phys. Colloq. **35**, C7-113 (1974).
[10] L. H. Jones, B. I. Swanson, and S. A. Ekberg, J. Chem. Phys. **81**, 5268 (1984).
[11] J. Friedel, R. Smoluchowski, and N. Kurti, "Chapter 6. Imperfect dislocations," in *Dislocations: International Series of Monographs on Solid State Physics* (Elsevier Science, 2013), ISBN: 9781483135922.
[12] Y. Adda, J. M. Dupouy, and J. Philibert, *Eléments de Métallurgie Physique: 3 Alliages et Défauts* (CEA, 1977), Chap. 22, ISBN: 2-7272-0014-5.
[13] B. Hammer, K. W. Jacobsen, V. Milman, and M. C. Payne, J. Phys.: Condens. Matter **4**, 10453 (1992).
[14] M. Ryan, M. Collier, P. dePujo, C. Crépin, and J. G. McCaffrey, J. Phys. Chem. A **114**, 3011 (2010).
[15] A. Masson, M. C. Heitz, J. M. Mestdagh, M. A. Gaveau, L. Poisson, and F. Spiegelman, Phys. Rev. Lett. **113**, 123005 (2014).
[16] J. A. Boatz and M. E. Fajardo, J. Chem. Phys. **101**, 3472 (1994).
[17] A. I. Krylov, R. B. Gerber, and R. D. Coalson, J. Chem. Phys. **105**, 4626 (1996).
[18] M.-C. Heitz, L. Teixidor, N.-T. Van-Oanh, and F. Spiegelman, J. Phys. Chem. A **114**, 3287 (2010).
[19] A. I. Krylov, R. B. Gerber, M. A. Gaveau, J. M. Mestdagh, B. Schilling, and J. P. Visticot, J. Chem. Phys. **104**, 3651 (1996).
[20] L. Balling and J. Wright, J. Chem. Phys. **79**, 2941 (1983).
[21] B. O. Roos, V. Veryazov, and P.-O. Widmark, Theor. Chem. Acc. **111**, 345 (2004).
[22] B. O. Roos, R. Lindh, P.-Å. Malmqvist, V. Veryazov, and P.-O. Widmark, J. Phys. Chem. A **108**, 2851 (2004).
[23] F. Aquilante *et al.*, J. Comput. Chem. **31**, 224 (2010).
[24] K. Abdessalem, L. Mejrissi, N. Issaoui, B. Oujia, and F. X. Gadea, J. Phys. Chem. A **117**, 8925 (2013).
[25] E. Czuchaj, F. Rebentrost, H. Stoll, and H. Preuss, Theor. Chem. Acc. **100**, 117 (1998).
[26] J. Rose, D. Smith, B. E. Williamson, P. N. Schatz, and M. C. M. O'Brien, J. Phys. Chem. **90**, 2608 (1986).
[27] M. A. Collier and J. G. McCaffrey, J. Chem. Phys. **122**, 054503 (2005).
[28] O. Byrne and J. G. McCaffrey, J. Chem. Phys. **134**, 124501 (2011).
[29] B. M. Davis, Ph.D. dissertation (Maynooth University, 2016).
[30] W. H. Breckenridge and C. N. Merrow, J. Chem. Phys. **88**, 2329 (1988).
[31] R. Pou-Amérigo, M. Merchán, I. Nebot-Gil, P. O. Widmark, and B. O. Roos, Theor. Chim. Acta **92**, 149 (1995).
[32] A. Kramida, Y. Ralchenko, J. Reader, and NIST ASD Team, NIST Atomic Spectra Database (version 5.3), available at: http://physics.nist.gov/asd, National Institute of Standards and Technology, Gaithersburg, MD, 20 July 2017.